THE TIME EXPANSION CHAMBER AS HIGH PRECISION DRIFT CHAMBER

A. H. Walenta
University of Siegen
Siegen, Germany

J. Paradiso*
Massachusetts Institute of Technology
Cambridge, Massachusetts, U.S.A.

H. Hofer, G. Viertel and J. Fehlmann
Eidgenössische Tech. Hochschule
Zürich, Switzerland

Abstract

With the principle of the time expansion chamber and the additional measurement of the position of the avalanche along the circumference of the anode wire it is possible to reconstruct the spacial distribution of the primary ionization in space. A position resolution for minimum ionizing tracks of $\sigma \lesssim 30$ μm is expected. First tests and concepts for vertex detectors are presented.

Introduction

Particles produced in high energy pp, $p\bar{p}$ and e^+e^- collisions are expected to consist of c, b and t quarks and have a relatively long lifetime, such that they come into the reach of identification by measuring their decay vertex separated from their production vertex. In order to detect these particles with a lifetime of $\tau \lesssim 10^{-13}$ a position resolution of $\sigma \lesssim 30$ μm is needed.

Earlier work[1] has shown that a drift chamber can reach a resolution which comes close to this value. The measurement was performed for several gases and mixtures for increasing pressure P and as a function of the drift length x. It was found that three main contributions to the position resolution σ can be distinguished:

$$\sigma^2 = A^2 + (\Delta x_{ion})^2 + (\Delta x_{diff})^2 \qquad (1)$$

The last term is due to diffusion

$$(\Delta x_{diff})^2 = \frac{2BD}{\mu E} x = 2B \frac{D}{\mu} \frac{1}{E/P} \frac{x}{P} \qquad (2)$$

with D the diffusion constant, μ the electron mobility, E the electrical field and B a correction factor which takes into account that a number of electrons participate in generating the stop signal. This contribution Δx_{diff} can be easily separated, because it becomes the main contribution for large x.

Δx_{ion} is a contribution due to the fluctuation of the primary ionization. Since a minimum ionizing particle leaves on its path through a gas only a few statistically distributed clusters of ionization ($\bar{n} \approx 10 \ldots 40$ cm^{-1}) at atmospheric pressure, the track looks microscopically fuzzy as can be seen from enlarged cloud or bubble chamber pictures. A drift chamber measures the position of the cluster with the shortest drift time to the anode (leading edge discrimination of the anode pulse) and therefore is sensitive to the random position of the cluster along the particle track.

Δx_{ion} depends on the mean distance between clusters $\lambda_{cl} = 1/\bar{n}$ with $\bar{n}$ the mean number/cm track length and therefore decreases proportionally with pressure.

The maximum of this contribution is at x = 0 with $\Delta x_{ion} = 1/2\ \lambda_{cl}$ and decreases rapidly with increasing x, a purely geometrical effect.

The constant contribution A was found to be independent of pressure, but different for different gases and mixtures. The lowest value A = 20 μm was found for a mixture of $C_2H_4 - C_3H_8$ (3:1). This effect could be due to the range of the primary electrons, fluctuations of the avalanche or resolution of the electronics.

The analysis of these data shows that it will be very difficult to improve the overall resolution further but indicates the basic problems. Therefore, a new type of chamber, the time expansion chamber,[2] has been investigated with respect to its application as a high precision vertex chamber which, in principle, corrects the limitations of the standard drift chamber described above, giving high position resolution already at atmospheric pressure and good double-track resolution at the same time. This type of chamber also opens the possibility for a position measurement of the second coordinate with the same high precision as in drift direction.

Principle of the Vertex Chamber

The best position resolution for the track of a minimum ionizing particle can be achieved if the position of each primary ionization cluster can be measured separately, and a straight (or slightly curved line in a magnetic field) is fitted through these points. Then the contribution Δx_{ion} as introduced above can be eliminated.

Furthermore, if the position of each cluster is measured separately, the measurement of the center-of-gravity of its spacial distribution after diffusion gives a precision of $\sigma_{cl} = \sigma_0/\sqrt{m}$, where σ_0 is the diffusion of a single electron and m is the number of electrons/cluster. If a total of n clusters is measured, the total contribution of the diffusion will be

$$\sigma = \sigma_0/\sqrt{m \cdot n} = \sigma_0/\sqrt{N} \qquad (3)$$

with $N = m \cdot n$ the number of electrons released in the track section under consideration. This represents a considerable reduction of the contribution of diffusion as compared to the method of leading edge discrimination. Also, the contribution A may be reduced if it is caused by the range of the primary electrons (for higher energy, called δ-rays) by rejecting the position measurement of "big" clusters, or if it is caused by fluctuations of the avalanche or the electronic timing by increasing the relative speed of the avalanche.

These improvements are in principle possible with a special readout of the time expansion chamber. There are two main features which distinguish this chamber from a standard drift chamber (Fig. 1)

(a) The drift region is separated from the gas amplification region by a fine grid. The electric field strength and gas mixture are adjusted to result in a small drift velocity (v_{Dr} = 5 μm/ns) as compared

*Now at ETH, Zürich, Switzerland.

to the usual value (v_{D_r} = 50 μm/ns). The full drift velocity is maintained in the gas amplification region and therefore the anode signal can follow the fluctuations of the primary ionization and even resolve individual clusters.

(b) Two pick-up wires are placed close to the anode wire. The difference signal is given by $\Delta PW \propto \sin\alpha$ with α the angle of the fieldline carrying the cluster to the anode as shown in Fig. 1. Since α determines the fieldline it also determines the coordinate y along the track.

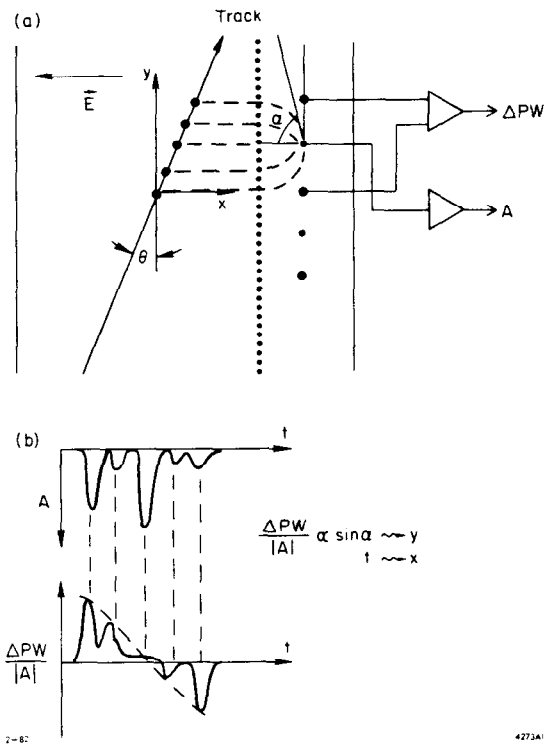

Fig. 1. Principle of time expansion chamber. (a) Layout with pick-up wires. (b) Signals.

Therefore, a track inclined with respect to the grid by an angle θ (Fig. 1) will allow the measurement of the individual clusters in two coordinates, x by the center-of-gravity of the drift time and y by determining α. For smaller θ the clusters will eventually merge and it will be difficult to eliminate large clusters and determine y. Still, the measurement of the center of gravity will result in an improved position resolution particularly since the y coordinate has less weight for smaller θ. Nevertheless, one may design the chamber layout such that a minimum angle θ is guaranteed (see Fig. 13).

A vertex detector is most effective close to the vertex and therefore a very good double-track resolution is of importance. The feature (a) of the time expansion chamber will automatically give a high double track resolution Δx only limited by the overlap of the projected track segments (Fig. 2) $\Delta x = d \cdot \tan\theta$ with d the segment in y direction accepted by an individual anode. At this point a compromise has to be found between position resolution ($\approx 1/\sqrt{d}$ because of the number of electrons N measured), a minimum θ for separating clusters, drift velocity and double track resolution.

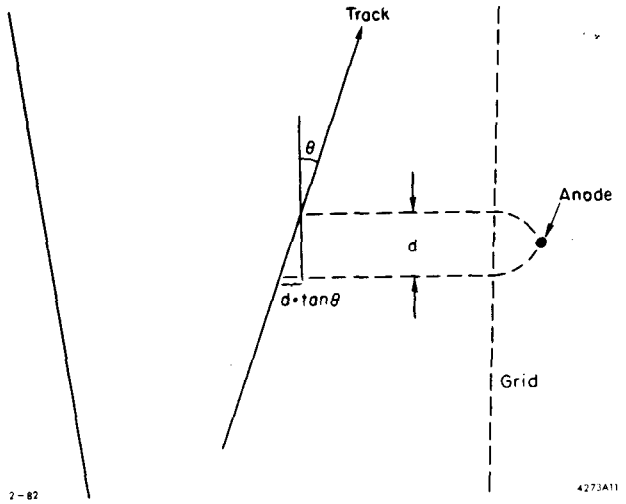

Fig. 2. Limit of double-track resolution due to the width of the projected ionization.

Measurements

Measurements have first concentrated on investigating the novel features of the time expansion chamber which lead to the reconstruction of the primary ionization.

The time expansion effect has been primarily introduced to accomodate the speed and response of the gas amplification to the time sequence of the arriving ionization. Therefore, it is convenient to discuss the time expansion chamber as a system (Fig. 3) consisting of a "delay line" (the drift space) connected to an "amplifier" (the "avalanche amplifier" plus electronic preamplifier). The "delay line" transforms the projection of a charge distribution ρ(x) into a time

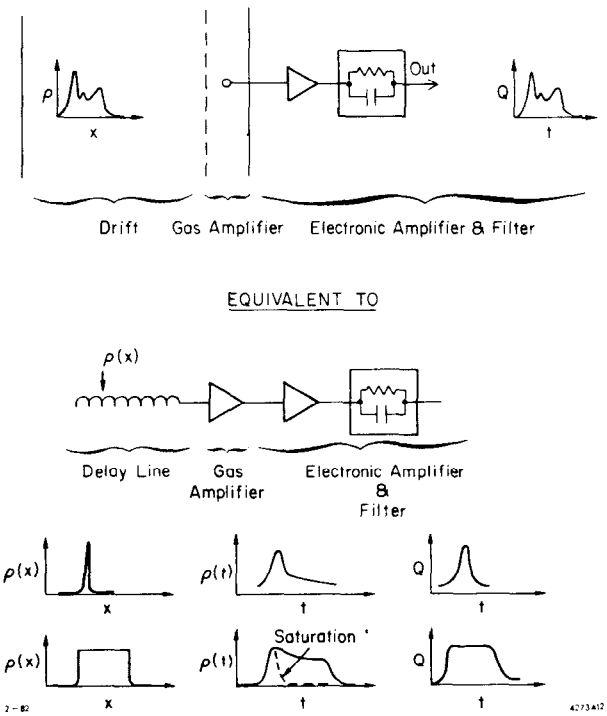

Fig. 3. The time expansion chamber and its electronic analogue; ρ(x) spacial distribution of charge, Q(t) signal.

sequence $\rho[x(t)]$ with $x(t) = v_{Dr} \cdot t$ and the amplifier transforms it into an electric signal $Q(t) = S\ \rho[x(t)]$ with S the amplification factor.

The "avalanche" amplifier and the electronic preamplifier are considered as one unit while the latter is assumed to cancel linear deformations of the "avalanche" amplifier by appropriate shaping (see, for example, Ref. 4).

Bandwidth of the Amplifier

Figure 4 shows the signal of one cluster produced by an ^{55}Fe X-ray in gain region behind the grid which can be considered as the response of the system to a δ-function $\rho(x - x_0) = \rho_0\ \delta(x - x_0)$. A width of Δt = 10 ns (fwhm) and almost complete cancellation of the tail has been achieved with the circuit shown. Sharper clipping reduced the amplitude without shortening the signal indicating the high frequency limit given by the "avalanche" amplifier.

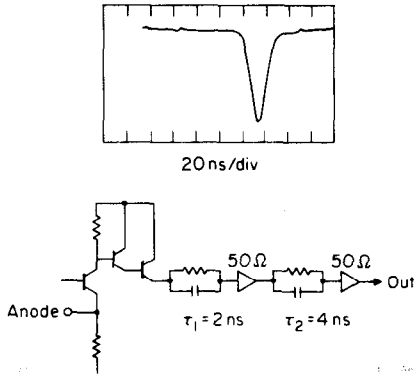

Fig. 4. Response to pointlike charge distribution (^{55}Fe). Grid to anode = 1.6 mm, ϕ anode = 20 µm.

Noise of the Amplifier

The noise of the "electronic" amplifier was a typical noise spectrum with an equivalent noise charge $\sqrt{ENC} = 5.10^3$ electrons (rms), a relatively high value. With a careful design of amplifier and chamber, better values can be achieved.[5] The noise of the "avalanche" amplifier would manifest itself in an amplitude variation which usually is identified as the energy resolution of the counter in the pulse mode. Also spurious signals would contribute to noise which could be expected as "after" pulses at high gain. By counting individual pulses in a pulse train for minimum ionizing particles as shown in Fig. 5, a plateau was reached for increasing gas gain, indicating that only ionization clusters contribute to signals. The mean number of measured clusters per track (the plateau-value) as a function of gas pressure shows that up to 1 atm no dead-time effects can be observed, which is interpreted as absence of nonlinear distortions (Fig. 6).

Drift Characteristics

The drift velocity has to be adjusted to v_{Dr} = 5 µm/ns, such that with the given bandwidth of the amplifier the spacial structure of roughly 50 µm of $\rho(x)$ can be recorded. This low drift velocity is obtained by operating with a drift field far below saturation, the mode which usually is used in drift chambers. The field is considered to be "low" if it has not yet heated up the electrons considerably and they are still close to thermal equilibrium. Then in good approximation one obtains[6] for the drift velocity

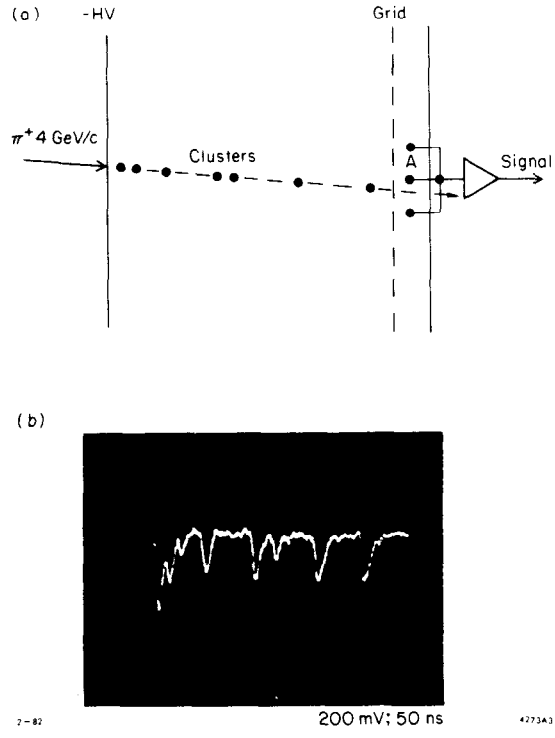

Fig. 5. Layout and signals for cluster measurement. Drift gap 10 mm, maximum drift time 1 µs.

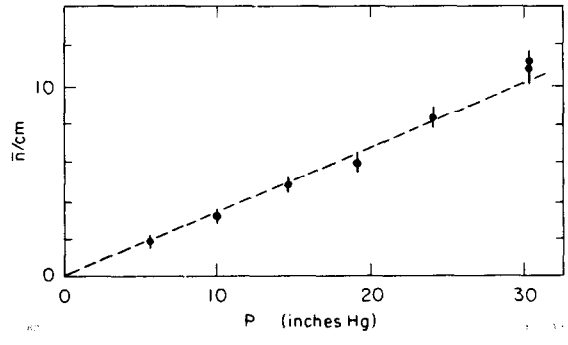

Fig. 6. Number of clusters/cm in 92% Ne + 8% methylal as a function of pressure.

$$v_{Dr} = \frac{2}{3}\ \frac{e}{m}\ \frac{E}{N}\ \frac{1}{\sigma \bar{v}} \qquad (4)$$

with N the gas density (molecules/volume), σ the momentum transfer cross section and $\bar{v}$ the mean electron velocity. It can be seen that the drift velocity increases under these conditions linearly with E/N, a result which is also important for calibration and stability (see below). Figure 7 shows the measured drift velocity for increasing concentration of methylal in argon which shifts this linear behavior to higher E/N.

Methylal has a large cross section for inelastic electron scattering and therefore tends to keep the electron energy in equilibrium with the gas. The diffusion coefficient is given by

$$D = \frac{1}{3}\ \frac{\bar{v}}{N\sigma} \qquad (5)$$

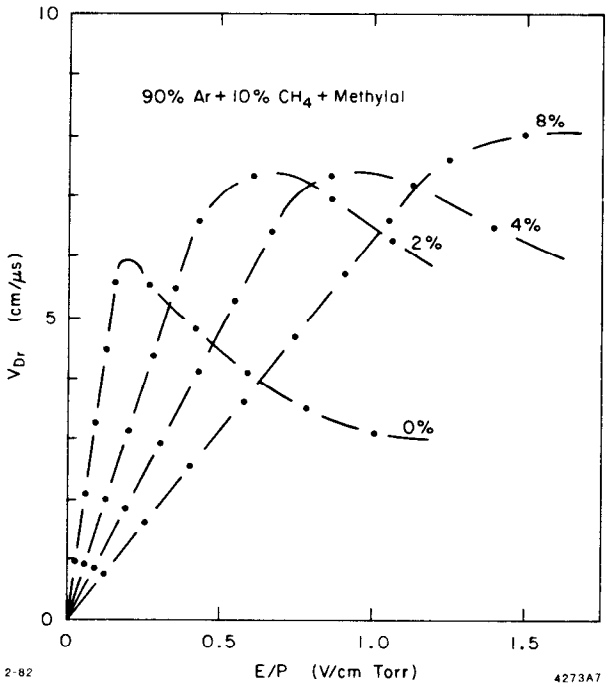

Fig. 7. Drift velocity of center of gravity (ionization from pointlike X-rays). The admixture of methylal is shown on the curves.

and together with the Einstein relation $\sigma = \sqrt{2Dt} = \sqrt{2D/v_{Dr}} \cdot x$ one obtains

$$\frac{\sigma^2}{x} = 2\,\frac{\varepsilon}{eE} \quad , \qquad (6)$$

where ε is the mean electron energy. For ε in equilibrium with the gas σ^2/x decreases ideally as 1/E, as shown in Fig. 8 (solid line). Measurements were performed with the time expansion chamber where the anode pulse width Δt was recorded from photographs and the diffusion determined by $\sigma = 0.43\, v_{Dr} \cdot \Delta t$. The standard drift gas (Ar + isobutane) shows very clearly a deviation from the ideal behavior (as expected[7]) while C_2H_4 + methylal gives lower values and follows to high E/N the diffusion data measured by different means.[8] This shows again that the anode signal follows the structure of $\rho(x)$ with a precision sufficient for the determination of the center-of-gravity of the signal.

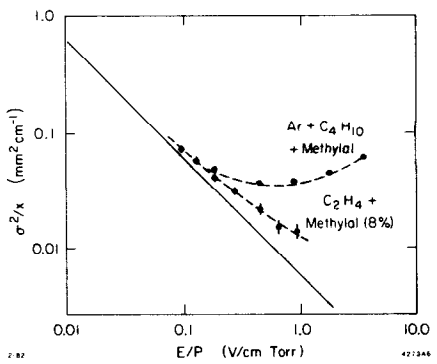

Fig. 8. Diffusion σ^2 for a drift length x as a function of E/P for P = 1 atm. Ar, C_4H_{10}, methylal from Ref. 7. Points with error bars measured in time expansion chamber; dashed line measured by Ref. 8 for C_2H_4.

Angular Measurement

The above mentioned feature (b), i.e., the angular measurement, has been tested with a cylindrical chamber without grid but with two pick-up wires close to the anode. X-rays (8 keV) have been used to simulate single ionization clusters under a given angle α. The difference signal has been clipped to a width of Δt = 20 ns (fwhm) and its amplitude spectrum recorded for different α (Fig. 9). The width of this distribution corresponds to an angular resolution of $\Delta\alpha$(rms) = 2.3°, partially due to the width of the collimation, limited mechanical accuracy or fluctuations in the avalanche. The resolution expected from the noise of the preamplifier[9] is negligible, namely $\Delta\alpha$(rms) = 0.8°.

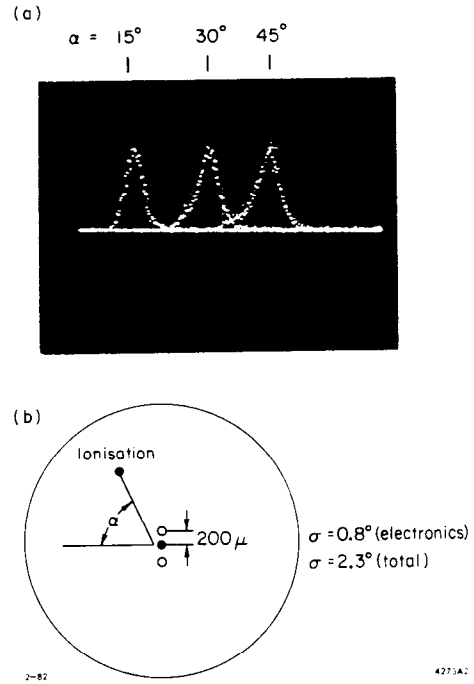

Fig. 9. (a) Pulse height distribution of difference signal ΔPW from pick-up wires for several values of α. (b) Electrode arrangement.

Double Track Resolution

An example of the double track resolution obtainable is shown in Fig. 10. The signals from three wires are displayed on the scope simultaneously by mixing them linearly after delaying two of them. γ-rays (bremsstrahlung from ^{106}Ru) occasionally produce pairs which are recognized by giving signals in two scintillators behind the chamber and two separate signals for the last wire. The central wire shows double signals too and a minimum distinguishable separation of Δx = 200 μm was found. This is in agreement with the expected diffusion, σ_{diff} = 70 μm for a drift length of x = 5 mm.

Readout

After amplification the anode signal (A) and the difference signal from the pick-up wires (ΔPW) are digitized with flash ADC's in 10 ns time samples and stored in 6 bit RAM's (1k memory)(Fig. 11). A prototype 512 bits deep has been tested successfully.[10] With drift velocity v_{Dr} = 5 μm/ns the sampling speed of Δt = 10 ns corresponds to σ = 15 μm, even if no center-of-gravity calculation is performed.

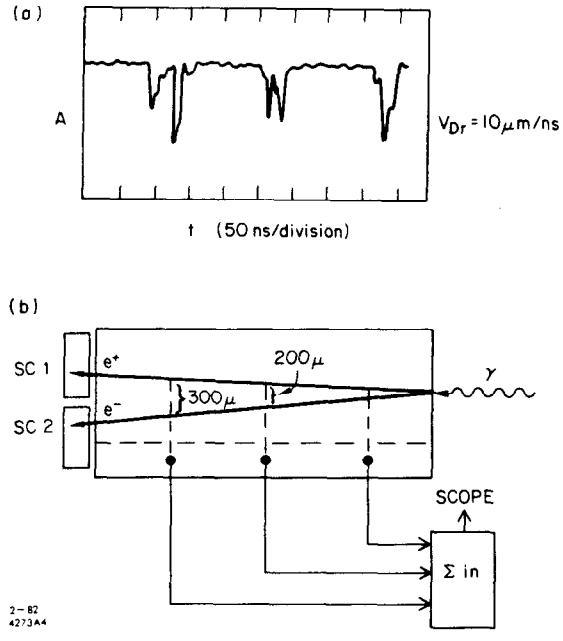

Fig. 10. (a) Signals from three anode wires displayed on scope. (b) Layout for measurement (Sc: scintillators).

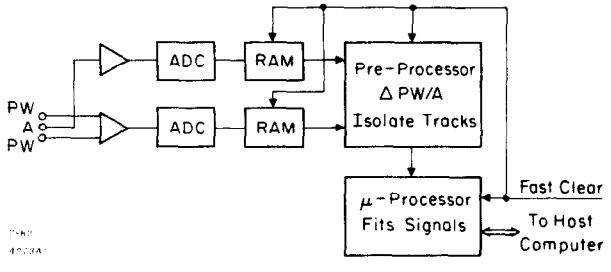

Fig. 11. Readout (schematically).

A preprocessor isolates and defines single track segments and calculates ΔPW/A. In principle, this information can be forwarded to the on-line computer but it may be convenient to process the data in dedicated μ-processors (one per wire) to increase computing power and reduce the amount of data written on tape.

Discussion

The reconstruction of the projection of the charge distribution $\rho(x)$ by measuring the pulse train $Q(t)$ is based on the assumption that the grid acts as a virtual amplification plane. This is achieved by a large time expansion factor where the drift velocity v_{Dr1} in the amplification zone is large compared to the value in the drift region v_{Dr2}, such that the longer drift path on field lines reaching the anode at large α becomes negligible. A time expansion factor of 10 (v_{Dr1} = 5 μm/ns, v_{Dr2} = 50 μm/ns) seems to be sufficient, but larger factors can be considered.

The fact that the chamber does not operate at saturated drift velocity turns out to be an advantage for the stability. The drift time for ionization in a point P(x,y,z) is given by

$$t_{Dr} = \int_x^{x_G} \frac{ds}{v(x,y,z)}$$

with x_G the position of the grid. Because of the choice of the gas we have

$$v_{Dr} = v_0\, E/N \qquad (7)$$

with v_0 depending on the gas mixture and E/N the reduced field strength. Furthermore, as long as the geometry of the chamber is unchanged $E(x,y,z) = U_0 F(x,y,z)$ with U_0 the applied high voltage and $F(x,y,z)$ a function depending only on geometry. Therefore, one obtains

$$t_{Dr} = \frac{N}{v_0 U_0} \int_x^{x_G} \frac{ds}{F(x,y,z)} \qquad (8)$$

Every measured drift time can be corrected with the same factor and only one point has to be monitored once the integral is known for each point from test beam measurements.

Another aspect of this detector is worth being mentioned. Once the cluster sequence has been measured from the anode signal, the measurement of the center-of-gravity on the pick-up wires would be sufficient to determine the exact location of the track, assuming its angle θ is known from the rough position measurement of other wires. This option would considerably reduce the electronics needed for readout.

The same principle offers the possibility of measuring the second coordinate (along the wire) with very high precision. From signal (Q) to noise (ΔQ) considerations, it can be shown that with proper design of amplifiers and detectors the readout of the center-of-gravity of induced signals on cathode strips (width d) can give a resolution[11]

$$\sigma = \frac{\Delta Q}{Q}\, d \sqrt{2 \sum_1^{k/2} n^2}$$

with $k \cdot d$ the width of the induced signal (about twice fwhm). A resolution of $\sigma \approx 15$ μm should be possible for d = 2 mm, $Q = 5.10^6$ and the chamber geometry of the time expansion chamber.

However, measurements and analysis of the data[12,13] show that limits of position resolution for minimum ionizing particles are determined by the fact that the center-of-gravity of the projected charge is measured and the latter is subject to large fluctuations. Only for $\phi = 0$ (Fig. 12) does this effect disappear.

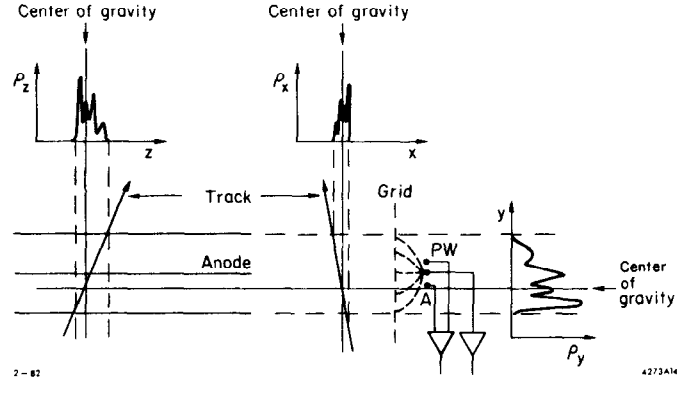

Fig. 12. Principle of three-dimensional center-of-gravity measurement. Coordinates as in Fig. 1. z along the anode wire.

Figure 12 also shows how the chamber described above can correct for these effects. A track crossing a gap

d and producing a charge distribution $\rho(s)$ (with s along the track) is shown in three projections. Depend- on the angles ϕ and θ these projections are linear images of each other. It follows then that the lines of back projections of the center-of-gravity of each view meet in a point which is exactly on the track.

This figure also illustrates the need for time expansion and shows two aspects. First, the time expansion must be large enough to allow the anode signal to follow the ionization structure in order to be able to determine its center-of-gravity. Second, it is the only measurement which can give the detailed structure. The measurement of the induced signals on the cathode strips or the pick-up wires gives a certain mean value which, for fine cathode strips, is the center-of-gravity but for the pick-up wires is given by

$$\overline{\Delta PW} \sim \int \rho_y \, g(y) \, dy$$

where g(y) includes the function mapping the field lines onto the circumference of the anode wire (angle α) and the function $\Delta PW \propto \sin\alpha$ producing the induced signals. For α not too large and careful design of the field lines g(y) approximately equals y and no further treatment is needed.* If these approximations are too coarse, the precise knowledge of ρ_x in drift direction can be used to obtain corrections. In this case the chamber geometry has to be arranged such that all tracks have $\theta \neq 0^o$.

Chamber Layout

A possible layout for a vertex detector around a beam pipe for intersecting storage rings is shown in Fig. 13. Here the individual cells have been tilted by 11.3° to guarantee inclined tracks for the high precision readout, particularly for the second

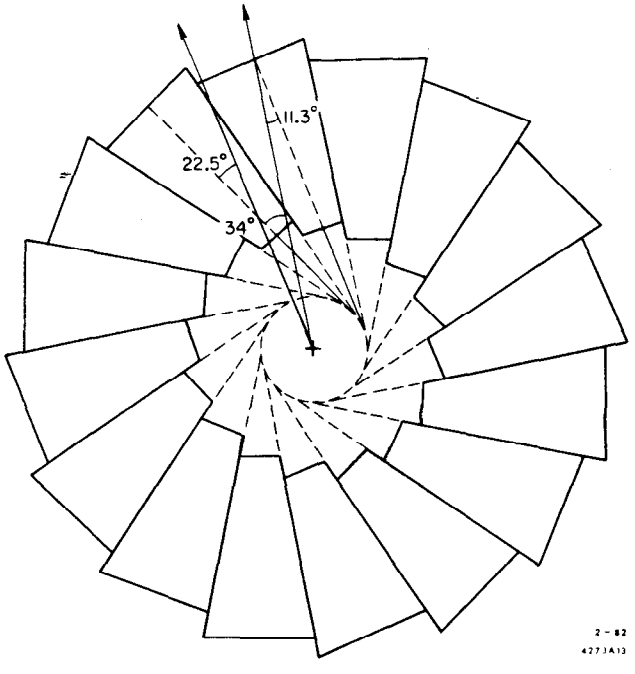

Fig. 13. Layout as vertex detector. Inner radius 6 cm, outer radius 17 cm; maximum drift path 2.6 cm.

coordinate. It may prove, however, that the gain in resolution is not large and then it will be more convenient to have the cells point to the center. This also would improve the double track resolution as discussed above.

In order to improve the pattern recognition, the high precision wires (with the readout of pick-up wires) have been interspaced with a pair of "pattern recognition" wires (Fig. 14) where d' = 1 mm is relatively small giving high double track resolution. They also resolve the right/left ambiguity. The position resolution of these wires will be roughly 100 μm in drift direction and 2 mm (rms) along the wires using charge division.

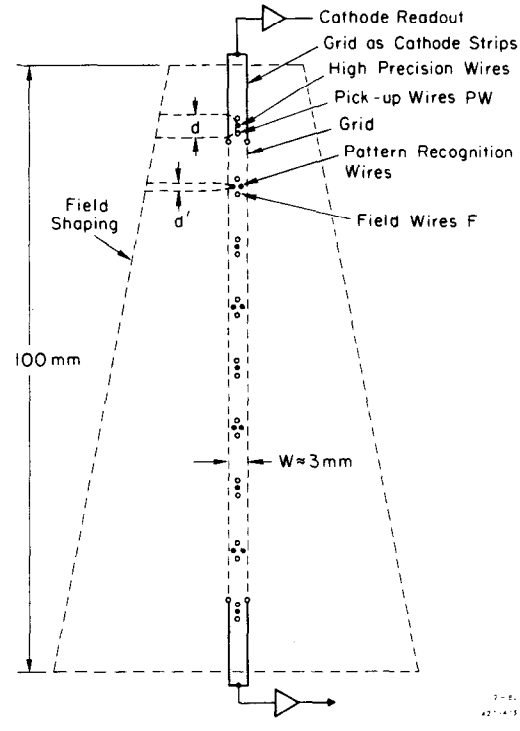

Fig. 14. One cell of vertex detector (schematically). Position of PW and F not to scale. F arranged to give d' = 1 mm. Double wire spacing 1 mm. Gap width w ≈ 3 mm, depending on d. Cathode strips at ends of separate frames serving as grid.

The innermost and outermost high precision wires are equipped with cathode strip readout for the high precision measurement along the wire. Since the chamber is relatively short (ℓ = 50 cm) a delay line split in five parts can be used in connection with the inner high precision wires (not shown) that can be designed for a precision of 50 μm (rms).

If this detector is mainly used for vertex reconstruction, a TPC-like geometry may be favorable. With a maximum drift length of 25 cm, a time expansion factor between 5 and 10 can be used and the three-dimensional reconstruction described above could give space points with typically 40 μm (rms). In addition, pressure would improve this value proportional to 1/P.

Conclusion

The time expansion chamber equipped with additional readout of induced signals allows, in principle, the reconstruction of the spacial distribution of the ionization of minimum ionizing tracks. The precision of the reconstruction seems so far to be limited only

*For a TPC detector, this would be a possibility to increase the precision of position measurement without time expansion.

by diffusion which can be further reduced by increasing the ionization density. Occasionally the range of the primary electrons may limit the resolution but little information is available up to now. The time expansion chamber may provide the missing data.

References

1. W. Farr, J. Heintze, K. H. Hellenbrand and A. H. Walenta, Nucl. Instrum. Methods, 154 (1978) 175.
2. A. H. Walenta, IEEE Trans. Nucl. Sci. NS-26 No. 1 (Feb. 1979) 73.
3. J. Fischer, H. Okuno and A. H. Walenta, IEEE Trans. Nucl. Sci. NS-25 (1978) 794.
4. R. A. Boie, A. T. Hrisoho and R. Rehak, IEEE Trans. Nucl. Sci. NS-28 No. 1 (1981) 603.
5. W. D. Farr and G. C. Smith, to be published.
6. See, for example, H.S.W. Massey and E.H.S. Burhop, "Electronic and Ionic Impact Phenomena," Oxford 1969.
7. V. Palladino and B. Sadoulet, LBL Report LBL-3013 (1974).
8. L. W. Cochran and D. W. Forester, Phys. Rev. 126 (1962) 1785.
9. The amplifier is a more recent design following the description given in "State of the Art of Low Noise Amplifiers for Semi-Conductor Radiation Detectors," V. Radeka, Proceedings of Int. Symposium on Nuclear Electronics, Versailles, 1968, Vol. I, page 46/I.
10. W. D. Farr, private communication.
11. See, for example, ISABELLE Proceeding of the 1978 Summer Workshop, BNL 50885, pp. 136-158.
12. C. H. Hargrove, private communication, and these proceedings.
13. A. E. Bondar, A. P. Onuchin, V. S. Panin and V. I. Telnov, "Spacial Resolution of the Induced Proportional Chambers," Preprint 82-017, Novosibirsk 1982.